

Transport simulations for W7-X

The results of transport modeling for both pure ECRH and pure NBI scenarios for the Wendelstein VII-X (W7-X) stellarator are presented. A set of calculations assuming neoclassical confinement plus anomalous contributions (dominant at low density and temperature) has been carried out for the standard magnetic configuration. The energy confinement time τ_E and its dependence on global plasma parameters are analyzed and compared with the prediction of the empirical scaling ISS04. Finally, W7-X performance is compared to that of a classical stellarator without elongation and with the same rotational transform, magnetic field, and minor and major radii.

Equations

To model transport in W7-X, we use a predictive one-dimensional (1-D) transport code [1]. The transport code is based on a system of equations, which consists of particle and power balance equations augmented by diffusion equations for the radial electric field and for the poloidal magnetic flux:

$$\begin{aligned} \frac{\partial n_e}{\partial t} + \frac{1}{V'} \frac{\partial}{\partial r} V' \Gamma_e &= S_p, \\ \frac{3}{2} \frac{\partial n_e T_e}{\partial t} + \frac{1}{V'} \frac{\partial}{\partial r} V' Q_e &= P_e - \Gamma_e E_r, \\ \frac{3}{2} \frac{\partial n_i T_i}{\partial t} + \frac{1}{V'} \frac{\partial}{\partial r} V' Q_i &= P_i + z_i \Gamma_i E_r, \\ \epsilon_0 \frac{c^2}{V_a^2} \left(1 + \frac{\beta_{10}^*}{I^2} \right) \frac{\partial E_r}{\partial t} - \frac{1}{V'} \frac{\partial}{\partial r} V' D_{Er} \frac{\partial E_r}{\partial r} &= |e| (\Gamma_e - z_i \Gamma_i), \\ \frac{\sigma}{2\pi R_0} \frac{\partial \psi_p}{\partial t} - \frac{1}{2\pi R_0 \mu_0} \frac{1}{V'} \frac{\partial}{\partial r} V' \frac{\partial \psi_p}{\partial r} &= j_{bs} + j_{cd} \end{aligned} \quad (1)$$

The neoclassical and anomalous fluxes in Eq. (1) are given by the expressions:

$$\begin{aligned} \Gamma_\alpha^{neo} &= -n_\alpha \left[D_{11}^\alpha \left(\frac{n'_\alpha}{n_\alpha} - \frac{z_\alpha E_r}{T_\alpha} \right) + D_{12}^\alpha \frac{T'_\alpha}{T_\alpha} \right], \\ q_\alpha^{neo} &= -n_\alpha T_\alpha \left[D_{21}^\alpha \left(\frac{n'_\alpha}{n_\alpha} - \frac{z_\alpha E_r}{T_\alpha} \right) + D_{22}^\alpha \frac{T'_\alpha}{T_\alpha} \right], \\ \Gamma_\alpha &= \Gamma_\alpha^{neo} + \Gamma_\alpha^{an}, \quad Q_\alpha = Q_\alpha^{neo} + Q_\alpha^{an}, \quad \alpha = e, i \\ Q_\alpha^{neo} &= q_\alpha^{neo} + \Gamma_\alpha^{neo} T_\alpha, \quad \Gamma_\alpha^{an} = -D_{ano}^\alpha n'_\alpha, \\ Q_\alpha^{an} &= -\chi_{ano}^\alpha n_\alpha T'_\alpha + \frac{3}{2} \Gamma_\alpha^{an} T_\alpha \end{aligned} \quad (2)$$

where n_α , T_α and Z_α are the density, temperature, and charge number of electrons or ions and the prime denotes the partial derivative with respect to the effective radius r . For evaluation of the transport coefficients D_{jk}^α we use a data set of transport coefficients calculated by the DKES [2] and GSRAKE [3] codes for the *standard* magnetic configuration and for different values of radial electric field, plasma radii, and collisionalities. The components of the transport matrix D_{jk}^α appearing in Eqs. (2) are a result of energy convolution of the monoenergetic coefficients with a Maxwellian distribution function.

ECRH scenarios, power and density scans

The ECRH scans are simulated for plasma densities $0.2 \times 10^{20} \text{ m}^{-3} \leq n \leq 10^{20} \text{ m}^{-3}$ using X2-mode heating (140 GHz at $B = 2.5$ T) with slightly off-axis deposition of power in the range from 2 MW to 10 MW. For the considered densities the X2-mode power is absorbed completely, and for simplicity we use a prescribed power deposition profile $P_{\text{ECRH}} \propto \exp[-(r-r_c)^2/w^2]$ with a 10-cm half-width. In the simulation we self-consistently determine the neoclassical fluxes and the radial electric field, which strongly affects the transport at low collisionality. The density is kept fixed and the equation for the poloidal magnetic flux is not used in these simulations.

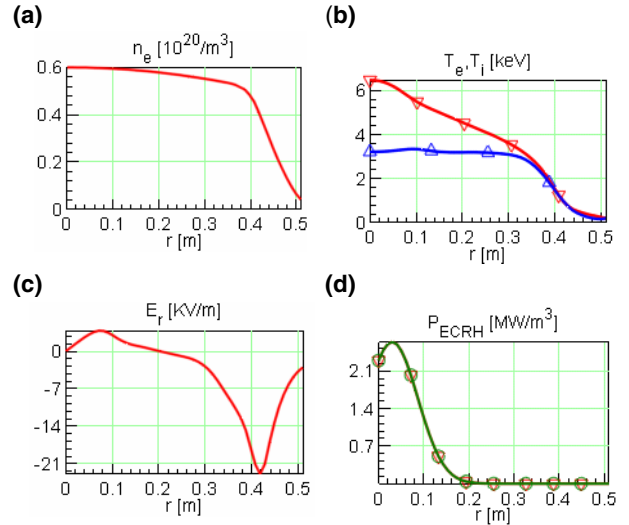


Fig. 1. Plasma profiles for the case of 3.32 MW of ECRH: (a) electron density; (b) electron (∇) and ion (Δ) temperatures; (c) radial electric field; (d) ECRH power deposition profile; $\tau_E = 0.517$ s.

Figure 1 shows the density and temperatures for the ECRH scenario along with the calculated radial electric field for a central density of $0.6 \times 10^{20} \text{ m}^{-3}$ and 3.32 MW of ECRH. In the plasma center, the “electron root” with a small positive electric field is seen. For lower density and the same heating conditions the electric field reaches higher values (up to 30 kV/m), while for higher density the “electron

root” disappears and the electric field becomes negative throughout the entire plasma.

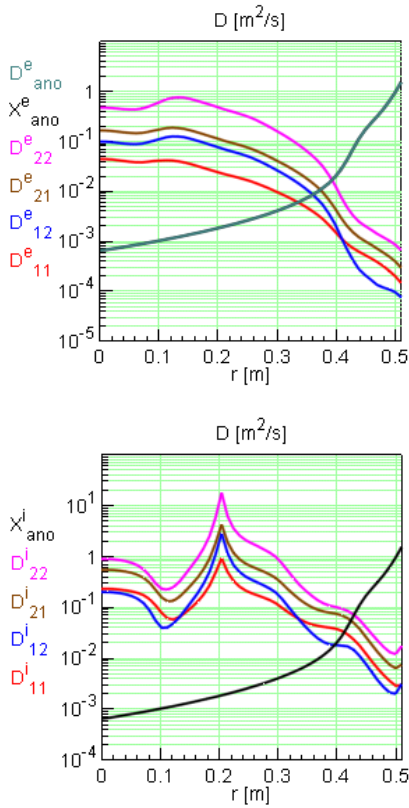


Fig. 2. (a) Electron and (b) ion diffusion coefficients; black curves are the anomalous heat diffusivities $\chi_{\text{ano}}^{\alpha}$, magenta curves are the neoclassical heat diffusivities D_{22}^{α} .

Corresponding to Fig. 1, neoclassical transport coefficients D_{jk}^{α} and anomalous heat conductivities $\chi_{\text{ano}}^{\alpha}$ are shown in Fig. 2. Based on the experience of high performance discharges of the W7-AS campaign [4] we choose the diffusion model to be neoclassical in the bulk plasma and anomalous at the edge. In the region of high density gradient the anomalous transport coefficients are taken in the form $D_{\text{ano}}^e = \chi_{\text{ano}}^e = \chi_{\text{ano}}^i \propto 1/n_e$ with exponential decay towards the center of the plasma. To maintain ambipolarity the relation $D_{\text{ano}}^e = D_{\text{ano}}^i$ is imposed.

Simulated confinement times τ_E for different ECRH powers and plasma densities are shown in Fig. 3. The energy confinement time scales with the plasma density as $\tau_E \propto \bar{n}_e^{0.8}$. Dependence on power is depicted in Fig. 3 (right); the confinement time is proportional to $P^{-0.5}$ for the low-density case and is $P^{-0.7}$ for the high-density case. The almost linear scaling of the energy confinement time with the plasma density is expected since both $1/\nu$ neoclassical transport and anomalous transport scale as $1/n$.

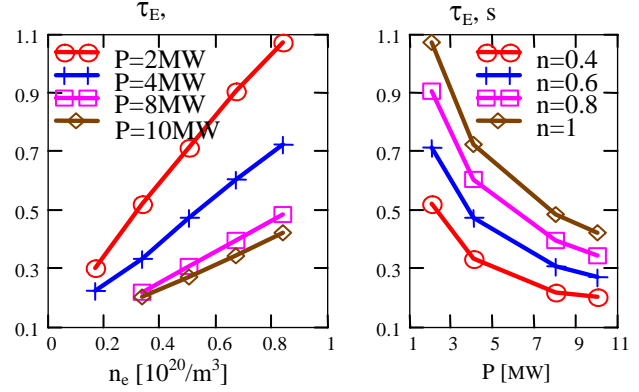


Fig. 3. Dependence of the energy confinement time on the line-average density (left) and on the ECRH power (right).

NBI heating scenarios, power and density scans

Power and density scans have been performed for the plasma heated by “positive” NBI (p-NBI, 60-keV H^+). Four beams launched through port AEK21 are used in the modeling. The beams have the same particle energy and power, with the power proportion $P_E:P_{E/2}:P_{E/3} = 50:30:20$ (i.e., fractions of the total input power carried by full-, half-, and third-energy neutrals). For modeling of NBI heating, a newly developed fast NBI module is used. The pencil-beam approach is used for the calculation of the birth profiles. The approximation of slowing-down of the fast NBI ions on the flux surfaces is used, allowing the use of a fast Fokker-Planck solver for evaluation of the power deposition profiles. The power deposition to ions and electrons is self-consistently calculated with the temperature profiles up to steady state. The density range is $0.5 \times 10^{20} \text{ m}^{-3} \leq n \leq 3 \times 10^{20} \text{ m}^{-3}$, where the lower limit is chosen to reduce shinethrough losses below 20%. The power is varied within $2 \text{ MW} \leq P \leq 10 \text{ MW}$.

Figure 4 shows NBI results for which the simulation parameters were chosen to have the same heating power as in the case shown in Fig. 1. The energy confinement time is almost the same as in the ECRH plasma, although the ion and electron temperatures are closer to each other and plasma neoclassical transport follows the “ion” root. In this case both electrons and ions are responsible for heat losses.

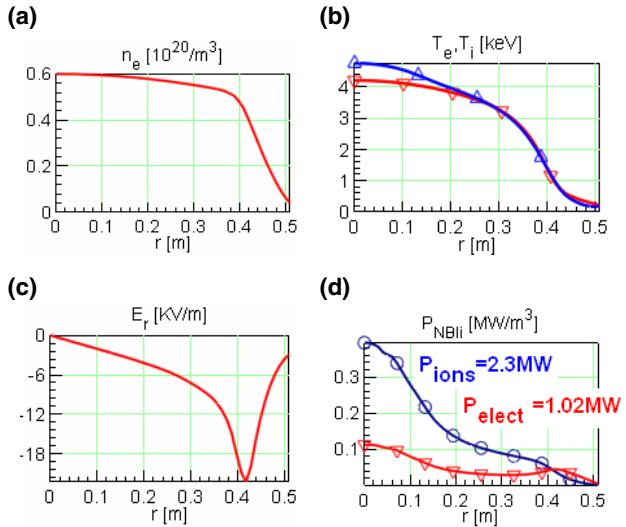


Fig. 4. Plasma profiles for the case of 3.32 MW of NBI heating: (a) electron density; (b) electron (∇) and ion (Δ) temperatures; (c) radial electric field; (d) NBI heating power deposition profiles; $\tau_E = 0.505$ s.

The simulated values of τ_E for different absorbed NBI powers and plasma densities are shown in Fig. 5. For densities lower than 10^{20} m^{-3} , the energy confinement time scales with the plasma density as $\tau_E \propto n_e^{0.54}$. At high densities the energy confinement time strongly decreases. Dependence on power is shown in Fig. 5 (right); the confinement time is proportional to $P^{-0.5}$ for the low-density case and $\tau_E \propto P^{-0.3}$ for the high-density case.

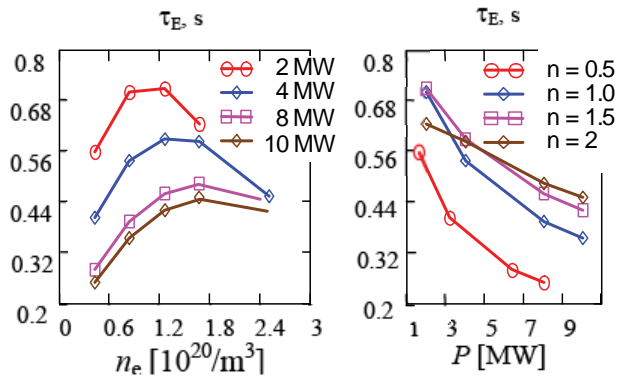


Fig. 5. Dependence of the energy confinement time on the line-average density (left) and on the absorbed NBI power (right).

In order to clarify the behavior of τ_E at high densities, a simulation of a dense plasma heated by a 150-keV hydrogen beam was performed. The results are presented in Fig. 6, which shows the high-density, high-power example for positive NBI (p-NBI, 60-keV H^+) and for negative NBI (n-NBI, 150-keV H^- , full energy only). In the p-NBI case, the

main power is absorbed at outer radii due to high densities at the edge. This leads to a τ_E degradation with density, whereas for the n-NBI case much higher central deposition allows for higher temperatures and improved global confinement. For example, $\tau_E = 0.45$ s and $\langle \beta \rangle = 4.2\%$ are obtained for p-NBI, with $\tau_E = 0.6$ s and $\langle \beta \rangle = 5.4\%$ for n-NBI. These simulation results demonstrate that confinement is not degraded by high densities; rather it is the NBI power deposition that is affected.

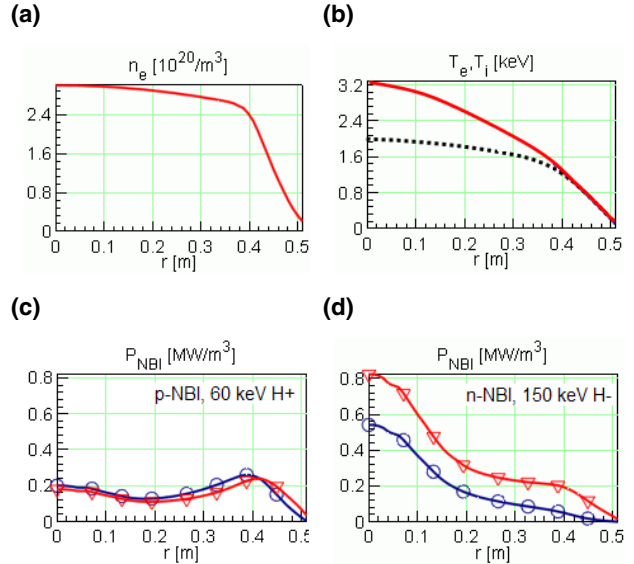


Fig. 6. (a) and (b): Plasma profiles for a 10-MW NBI predictive 1-D simulation of W7-X. The dotted line in the temperature figure refers to the p-NBI power deposition shown in plot (c) and the solid line refers to the n-NBI power deposition in plot (d).

Dependence on anomalous transport

The outcomes of transport simulation show a rather high value of the energy confinement time, and naturally a question arises as to the strength of the dependence of the results on anomalous transport. A sensitivity analysis of W7-X performance has been done for 4 MW of ECRH, a central density of $0.6 \times 10^{20} \text{ m}^{-3}$ and several models of anomalous diffusivity: $\chi_{\text{ano}}^\alpha = 0.014/n$, $0.07/n$, and $0.35/n$. Figure 7 shows the dependence of plasma parameters on the value of anomalous heat diffusivity at the plasma edge. The points on the plots correspond to the above-mentioned anomalous diffusivities. The results demonstrate a weak dependence of the plasma parameters on the level of anomalous transport; τ_E decreases by a factor of 1.8, whereas the anomalous heat diffusivity increases by 25 times.

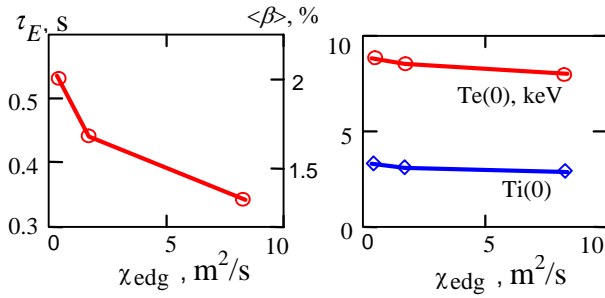


Fig. 7. Dependence of τ_E , $\langle\beta\rangle$, $T_e(0)$, and $T_i(0)$, on the edge value of anomalous heat diffusivity.

Central electron and ion temperatures are affected only slightly—both temperatures decrease by 10%; therefore the core transport does not depend on the plasma edge transport. Such behavior of the transport is explained by the anomalous diffusion model used: it is local and does not necessarily influence the core transport. This choice of anomalous model is supported by W7-AS campaigns [5] where it was observed that the central transport is not affected by the edge transport and profile stiffness was never seen. For the highest level of anomalous transport, the temperatures are nearly zero for the last 18% of the plasma radius and we may conclude that degradation of W7-X performance is simply caused by a decrease in plasma volume; see Fig. 8.

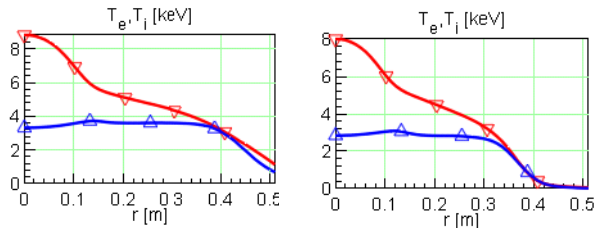


Fig. 8. Temperature profile for different anomalous heat diffusivities; left: $\chi_{\text{ano}}^{\alpha} = 0.014/n$, right: $\chi_{\text{ano}}^{\alpha} = 0.350/n$.

W7-X and ISS04

The results of density and power scans for both ECRH and NBI simulations are compared with ISS04 scaling $\tau_E^{\text{ISS04}} = 0.465a^{2.28}R^{0.64}P^{-0.61}n^{0.54}B^{0.84}\tau_{2/3}^{0.41}$. In Fig. 9 the values of τ_E from W7-X simulations are added to experimental data from the International Stellarator Confinement Database (ISCDB).

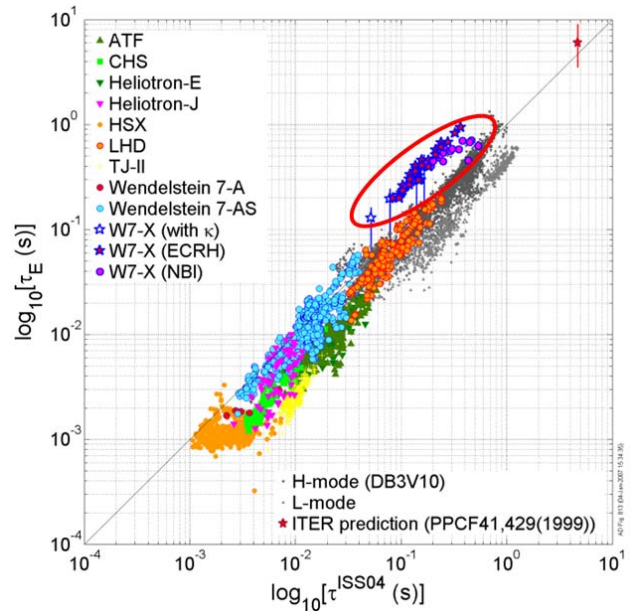


Fig. 9. Experimentally observed energy confinement times and results from neoclassical simulations for W7-X versus ISS04. The degradation of τ_E for NBI is due to the outward shift of the power deposition with increasing density.

The predicted confinement time are shown inside the red ellipse in Fig. 9. Our results demonstrate longer confinement time than that expected from the ISS04 scaling due to the predominance of neoclassical transport. This is consistent with the results of W7-AS campaigns, in which it was shown [4] that confinement was neoclassical in nature for high-performance discharges and that such W7-AS discharges had better confinement than predicted by the ISS95 scaling [5]; see also the W7-AS data in Fig. 9. Strong neoclassical transport optimization leads to further improvement of the plasma confinement in W7-X, consistent with the impact of the high W7-X elongation as described in the ITER ELMy H-mode scaling for tokamaks [6].

W7-X and classical stellarator

The same set of calculations has been performed for a classical stellarator. As a reference model, a classical stellarator without elongation and with the same rotational transform, magnetic field, minor and major radii as W7-X has been modeled. In Fig. 10 the results are summarized and compared with ISS04 predictions. The closed symbols in Fig. 10 correspond to W7-X (the same data as in the red ellipse in Fig. 9); the open symbols stand for the reference stellarator. The classical stellarator results are slightly higher than predicted by ISS04. The energy confinement times for W7-X are about twice as high as those for the classical stellarator.

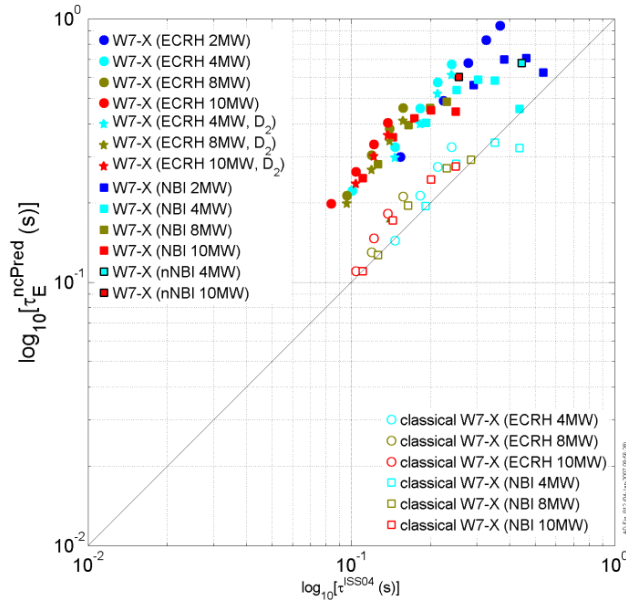


Fig. 10. Neoclassical predictions of energy confinement times for W7-X (closed symbols) and for the classical stellarator (open symbols) versus ISS04.

Summary

We have studied the energy confinement properties of W7-X assuming neoclassical diffusion in the bulk plasma and anomalous diffusion at the edge. Modeling has shown that the energy confinement time demonstrates a complex dependence on plasma parameters. In order to effectively heat plasma at high density ($2 \times 10^{20} \text{ m}^{-3}$ and higher), 150-keV hydrogen neutrals are needed, which implies the necessity for a source of negative hydrogen ions. For most cases considered in this paper the confinement times are higher than predicted by ISS04. We attribute this improvement to the neoclassical transport optimization in W7-X. The neoclassical predictions described here give an upper limit of plasma performance in W7-X. The same set of calculations has been done for a similar classical stellarator and the results have been compared with ISS04 predictions. The results for a classical stellarator are in good agreement with the ISS04 scaling. The energy confinement time for W7-X is about two times higher than that for a classical stellarator with the same dimensions but without elongation.

It is planned to continue self-consistent 1-D transport simulations for different magnetic configurations and heating scenarios of W7-X to create a reference profile database which is needed for various purposes, for example, for calculations of neutron production and for the development and testing of diagnostics software.

Acknowledgements

The authors gratefully acknowledge valuable discussion from F. Wagner and permanent support by the W7-X team.

Yu. Turkin, C. D. Beidler, A. Dinklage, J. Geiger, H. Maaßberg, N. B. Marushchenko, and the W7-X Team
 Max-Planck-Institut für Plasmaphysik, EURATOM-Association,
 Greifswald, Germany
 E-mail: yuriy.turkin@ipp.mpg.de

References

- [1] Yu. Turkin et al. *Fusion Sci. and Technol.* **50**, 387 (2006).
- [2] W. I. van Rij and S. P. Hirshman, *Phys. Fluids B* **1**, 563 (1989).
- [3] C. D. Beidler and W. D. D'haeseleer, *Plasma Phys. Control. Fusion* **37**, 463 (1995).
- [4] H. Maaßberg et al., *Phys. Plasmas* **7**, 295 (2000).
- [5] F. Wagner et al., *Phys. Plasmas* **12**, 072509 (2005).
- [6] ITER Expert Group, *Nucl. Fusion* **39**, 2204 (1999).

Editor's announcement

I have decided to jog the schedule for *Stellarator News* by a month to avoid the year-end holiday period. Hence this issue is out in February rather than January. The next issue will be in March.

I welcome submissions for *Stellarator News* from any reader. Please send them to me, James Rome at jar@ornl.gov.